

Automatic Correction of Machining Reference Plane Level to Improve the Processing Quality of Six-axis Robotic Arms

Yuan-Ming Cheng,^{1*} Yu-Hao Chang,² and Yu-Jie Weng²

¹Department of Intelligent Robotics, National Pingtung University, Pingtung 90004, Taiwan, Republic of China

²Department of Computer Science and Information Engineering, National Pingtung University, Pingtung 90004, Taiwan, Republic of China

(Received November 11, 2024; accepted April 10, 2025)

Keywords: robotic arm, mechanical probe, automatic measurement, datum correction, relief processing, flatness

Robotic arms are frequently used in automated machining to enhance production efficiency. The tool position is often determined with respect to a machining reference plane. If this plane is not level, machining precision may decrease. However, most researchers have focused on measuring machine tool lengths to improve tool position measurements; few have investigated correcting the levelness of the machining reference plane. In this study, an automatic method for plane correction was developed. A robotic arm equipped with a mechanical probe was used to measure locations on the machining reference plane, and its deviation angle was calculated. These data were then input to the RoboDK software for the correction of the machining reference plane, the accuracy of which was validated by measurements along an S-shaped path over the machining reference plane, and both the flatness and range of the measured points were used as evaluation metrics. Finally, actual engraving was conducted to confirm the quality of the robotic arm machining.

1. Introduction

In the relentless pursuit of automation and efficient production in modern manufacturing, robotic arms play an increasingly critical role as a vital component of automation systems.⁽¹⁾ Robotic arms are commonly used for tasks requiring high repeatability and precision, such as assembly, welding, inspection, and packaging,^(2,3) and are also applied in medical engineering.⁽⁴⁾ This not only considerably enhances production efficiency but also reduces the error rate associated with manual operations. The versatility and high controllability of robotic arms enable them to perform various tasks on the production line. However, before leveraging these advantages, it is essential to know the spatial position of the robotic arm, particularly the length of the machining tool. Thus, the automatic positioning of the tool center point (TCP) of the robotic arm is a method widely used to determine the tool's center position in precision machining and manufacturing processes.

*Corresponding author: e-mail: Chengym@mail.nptu.edu.tw
<https://doi.org/10.18494/SAM5476>

To enhance the absolute positioning accuracy of industrial robots, numerical compensation for positioning errors predicted using the Denavit and Hartenberg (D–H) model⁽⁵⁾ has been extensively studied. Alam *et al.*⁽⁶⁾ reviewed the kinematic modeling theory of six-axis industrial robots, provided a tutorial for readers on the derivation of kinematic models for six-axis robots, and proposed models equivalent to the classical D–H model that can be derived using different definitions of the local coordinate system.

A common method for conventional manual calibration involves using the machining tool to touch a sharp calibration rod. The operator moves the TCP to the tip of the calibration rod and adopts four or more different postures for the tool center point position (TCPP) in four distinct positions. Subsequently, at least one point is selected on each axis of the TCP frame, and the TCPP obtained through calibration is set as the origin and then moved to the tip, thereby establishing the tool center point frame (TCPF). The conventional method of marking the TCP mainly involves aiming the TCP at reference points in different postures, which are recorded by the robot arm's controller. However, this process is both time-consuming and labor-intensive. To reduce manual errors, Lin *et al.*⁽⁷⁾ and Lin and Wang⁽⁸⁾ proposed an automatic calibration method for the TCP on a six-degree-of-freedom collaborative robot using a laser displacement sensor. Hallenberg⁽⁹⁾ introduced a new method for the automatic iterative calibration of industrial robots' TCP using computer vision and image processing technologies, automatically executing a four-point TCP calibration algorithm.

Zhang *et al.*⁽¹⁰⁾ developed a specialized binocular vision system and introduced a vision-based TCP calibration algorithm that simultaneously identifies the TCPP and TCPF. The proposed method, characterized by high accuracy and stability, contributes positively to the clinical application of high-precision robot-assisted puncture surgeries. Liu *et al.*⁽¹¹⁾ proposed an automatic calibration algorithm for the robot TCP based on binocular vision measurement. A binocular vision sensor attached to the robot TCP is used to recognize targets. By constraining the measurement with binocular vision in three-dimensional space and combining multiple translational movements of the robot's end tool, the pose transformation between the vision sensor and the robot base can be calculated. Fares *et al.*⁽¹²⁾ introduced a TCP calibration method for industrial robots based on the sphere fitting method, a calibration method using the results of the four-point calibration method as initial data, to avoid precise point-to-point matching operations associated with low-cost multi-point calibration methods. Borrmann and Wollnack⁽¹³⁾ proposed a TCP calibration method based on a laser tracker. They designed a system using a laser tracker and two tool spheres that can reflect the laser beam, and installed this measuring system on the TCP. By rotating the robotic arm and recording the tool spheres' information with the laser tracker, the actual TCP can be determined by a homogeneous transformation matrix.

Xue *et al.*⁽¹⁴⁾ introduced a novel automated method for the precise calibration of industrial robots' TCP using the IONA system, an expandable network of photogrammetry sensors. The method consists of a portable TCP cube device, a workpiece mounted on the robot's end effector, and the IONA system. Kuric *et al.*⁽¹⁵⁾ described the use of a dual-sphere gauge device (Renishaw ballbar QC20-W) for measuring industrial robots. It employs circular motion paths on inclined planes for measurement, providing extensive information about the current technical state of the robot. Bergström⁽¹⁶⁾ used a standard method that utilized a spherical probe tool and calibration

cup for the TCP calculation. Cai *et al.*⁽¹⁷⁾ proposed an innovative solution for robot unit calibration using touch screens, an easily accessible and cost-effective device commonly used on tablets and smartphones.

Common methods for the automatic positioning of robotic arms' TCP include sensor and feedback systems, vision systems, mechanical probes, sound or ultrasonic positioning, magnetic positioning, automatic calibration, learning algorithms, and robotic arm dynamic simulation. Mechanical probes are particularly favored for their high accuracy, speed, reliability, applicability, and ease of implementation, making them the most widely used tools.^(18,19) The feedback from mechanical probes can be used to adjust the motion of the robotic arm, accurately locating the position of the tool.

In the manufacturing process, ensuring that the workpiece is in the correct position and orientation is a key factor in guaranteeing product quality. To achieve a rapid and precise correction of the workpiece's horizontal position, the application of robotic arms in conjunction with mechanical probes has become a notable solution. However, when it comes to the horizontal correction of workpieces, ensuring their accurate and immediate adjustment to the ideal position presents a challenge. In this context, the introduction of mechanical probes has brought new possibilities to this process.

Mechanical probes are capable of detecting the relative position of a workpiece's surface in real time and determining its levelness through high-precision measurements. In this study, we focus on the use of robotic arms in conjunction with mechanical probes for workpiece level correction and discuss the potential advantages of this technique, including improved accuracy, reduced error rate, and increased automation. We aim to provide users with insights into the technical characteristics of using robotic arms paired with mechanical probes for workpiece level correction, as well as the practical benefits this application brings to the manufacturing industry, offering valuable references for the development of future automated manufacturing.

2. Experimental Setup

Robotic arms have the capability for high-speed, stable operations, enabling them to swiftly execute tasks with high repeatability and precision. This substantially shortens the production cycle and enhances overall production efficiency. Robotic arms are widely used in the field of automated processing. When robotic arms are applied in machining, the machining reference plane is generally assumed to be level; however, this is often not the case. The machining reference plane is related to the base values of the machined workpieces. If the machining reference plane is not corrected for its basic levelness, it undermines the robotic arm's machining precision. However, most researchers focus on performing machining after measuring and compensating for tool lengths, neglecting the correction of the machining reference plane.

To accurately correct the machining reference plane, in this study, we developed an automatic measurement method using a robotic arm. The method involves mounting a mechanical probe on the robotic arm to measure the machining reference plane. After calculating the deviation angle of the reference plane, the data are input into the RoboDK software to correct the machining reference plane. Below is the architecture of the automatic measurement system.

2.1 Architecture of proposed automatic measurement system

Table 1 shows the components constituting the automatic measurement system in this study, including a six-axis robotic arm, a human-machine interface (HMI), a mechanical probe, a programmable logic controller (PLC), and ten relays. Figure 1 shows the architecture of the automatic measurement system. The PLC is the main controller, and the HMI is designed with buttons to initiate measurements and other functions. It also stores probe measurement data. A relay adapter board was produced with ten relays for signal exchange with the general-purpose I/O base boards CN308 and CN309 in the robotic arm’s control box. Measurement paths were planned using the RoboDK software and then input into the robotic arm’s teaching box. The mechanical probe was the CITIZEN SA-S110; it had a measuring working range of 10 mm, a minimum readout of 0.1 μm , and an indication accuracy of up to 0.1 μm .

Table 1
Components constituting the automatic measurement system.

Name	Six-axis robotic arm	HMI	Mechanical probe	PLC	Relay
Model type	YASKAWA MH5LF	DELTA DOP-107IV	CITIZEN SA-S110	DELTA DVP28SV11T2	Omron LY2-DC24

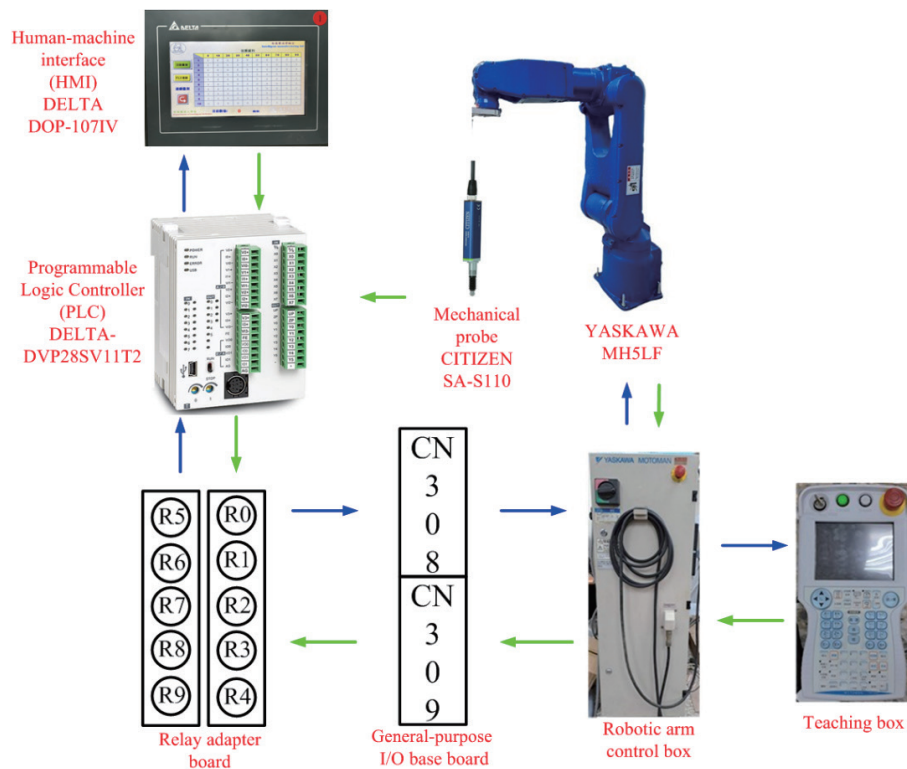


Fig. 1. (Color online) Architecture of automatic measurement system.

2.2 Measurement program

Figure 2 shows a flowchart of the programs for measurement in four parts, namely the HMI, the PLC, Autodesk Inventor, and RoboDK, and the programs are input into the robotic arm's teaching box.

The PLC is the host of the automatic measurement system and has two modes: reversion and measurement. The PLC enters the reversion mode when it is powered on or the homing button on the HMI is pressed. The machine then resets before entering the measurement mode. Measurements begin when the M1 button on the HMI is pressed; the arm then returns to a safe state (M60), and the continuous measurement mode (M10) is deactivated. For the robotic arm to complete the automatic measurement program, the PLC must be integrated with the teaching box path for overall planning.

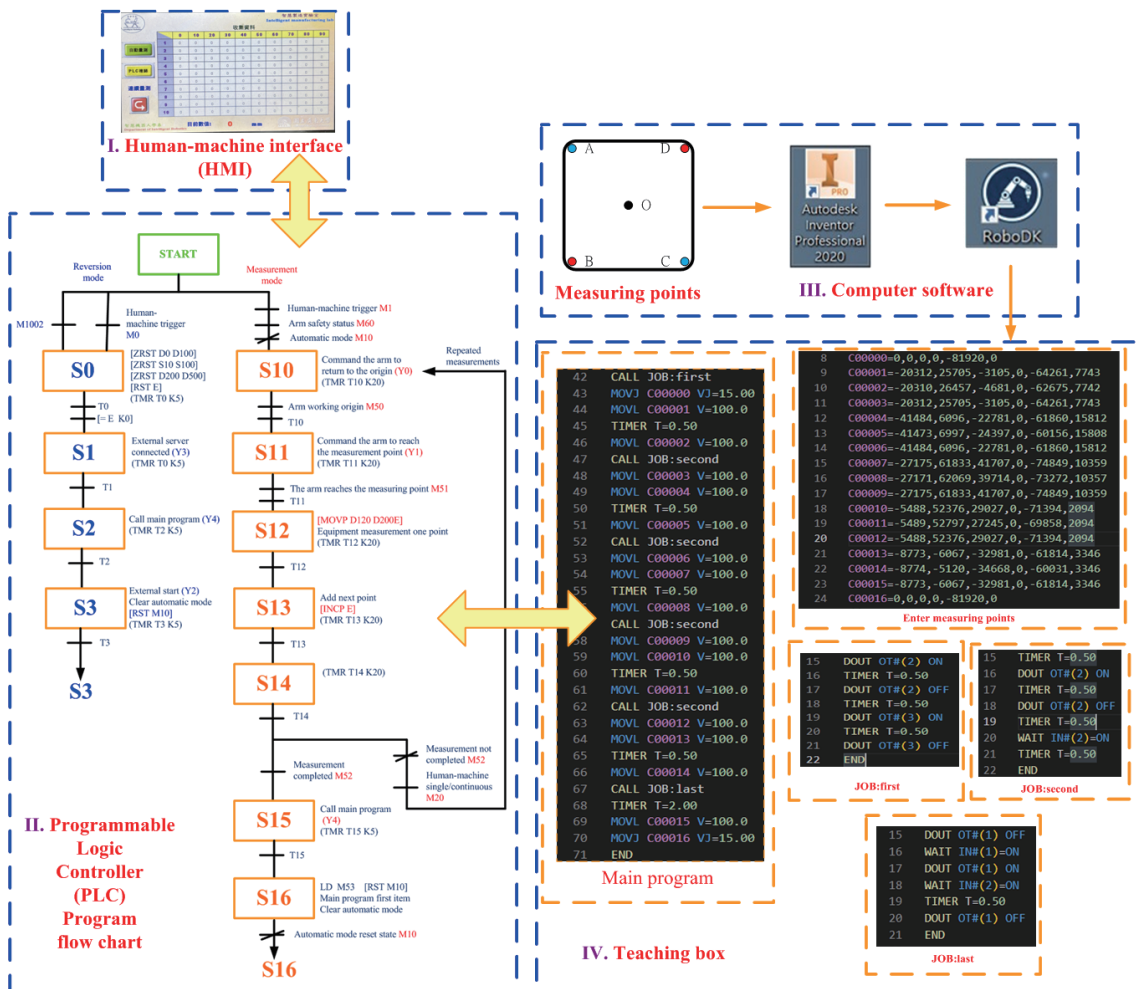


Fig. 2. (Color online) Flowchart of measurement program.

The PLC communicates with the robotic arm's teaching box by exchanging signals through the relay adapter board and the general-purpose I/O base boards CN308 and CN309 in the robotic arm's control box. The teaching box program comprises five parts: the main program, entering measurement points, subroutine 1 (JOB:first), subroutine 2 (JOB:second), and subroutine 3 (JOB:last). The main program controls the six-axis robotic arm's movement positions (measurement points), direction, and speed; it also calls subroutines 1 to 3.

Subroutine 1 (JOB:first) starts up the arm, activates its servos, executes the first item of the main program, and defines the robotic arm's working origin and other I/O points. Subroutine 2 (JOB:second) manages the mechanical probe's measurement signal, displays the measurement data on the HMI, and stores the data in the HMI's registers. Subroutine 3 (JOB:last) obtains the signal for the final measurement position by the mechanical probe and signals the PLC when all point measurements have been completed.

The PLC then ends the measurement program and enters status point S15. It then calls the main program and exits the automatic mode, returning to the first line of the main program in a standby state.

3. Experimental Methods

If the machining reference plane is not level, machining quality may decrease. To correct the levelness of the work surface, measurements were first performed at five points (Fig. 3) and then along an S-shaped path (Fig. 4) over the entire work surface. Both flatness and range methods were used to characterize the machining plane.

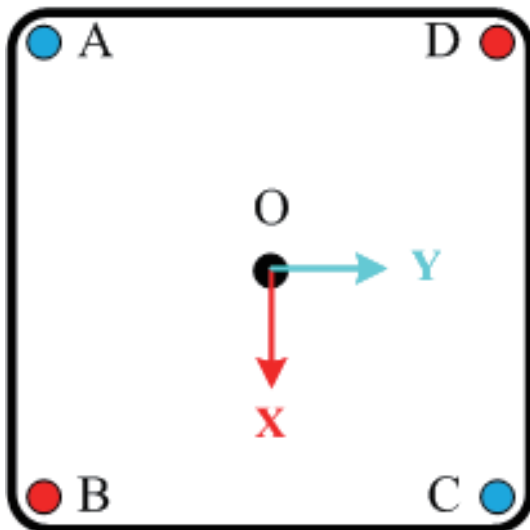


Fig. 3. (Color online) Five measurement points.

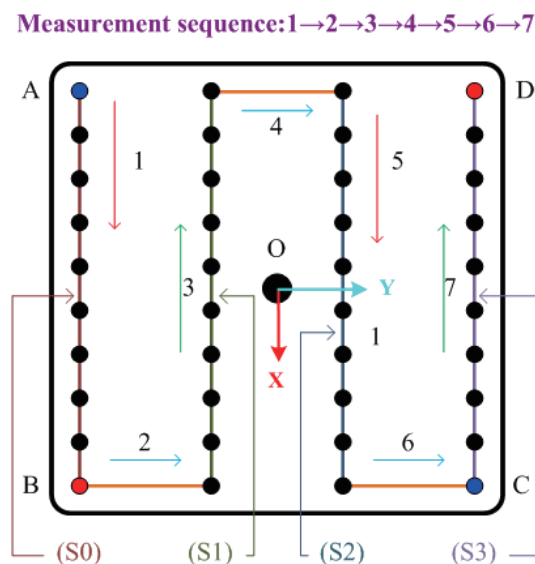


Fig. 4. (Color online) S-shaped measurement path.

3.1 Work surface correction

Figure 5 shows the correction process for the work surface. First, the Z values of four corner points and the central point of the plane were measured (Fig. 3). These measurement points were then programmed into RoboDK before being imported into the robotic arm's teaching box. The automatic measurement process was performed as illustrated in Fig. 2 and described in Sect. 2.2. The values measured by the probe were recorded on the HMI and then imported into Excel software to calculate the differences in elevation between points A, B, C, D, and the central point O. The differences between the pairs (A and C) and (B and D) were then assessed to determine if an excessive discrepancy exists between either set of points considering that CITIZEN SA-S110, the adopted mechanical probe, has a measuring working range of only 10 mm. If the differences in values were very large, the angles of inclination relative to the central point (Fig. 5) for both sets of points (A and C, B and D) were calculated, and their average values were determined. These average values were then used to compile a new measurement program based on new user coordinates. If the differences fell within the range of the mechanical probe, additional measurement points (such as on the S-shaped path shown in Fig. 4) could be added to comprehensively measure the work surface.

3.2 Flatness

A surface's flatness can be defined as the minimum distance between two parallel planes to contain all points on the surface. Flatness is often calculated by the least-squares method to identify the plane with the minimal sum of the squares of the residuals between the plane and the measured points. In general, a plane can be represented as

$$z = ax + by + c, \quad (1)$$

where a , b , and c are parameters that represent the plane's slope and intercept. The goal is to find the optimal values of a , b , and c that minimize the sum of squared residuals:

$$S = \sum_{i=1}^N (z_i - ax_i - by_i - c)^2, \quad i = 1 - N. \quad (2)$$

We first took the partial derivatives of S with respect to a , b , and c , set them equal to zero, and solved for the values of a , b , and c .

$$\begin{cases} \frac{\partial S}{\partial a} = -2 \sum_{i=1}^N (z_i - ax_i - by_i - c)(-x_i) = 0 \\ \frac{\partial S}{\partial b} = -2 \sum_{i=1}^N (z_i - ax_i - by_i - c)(-y_i) = 0 \\ \frac{\partial S}{\partial c} = -2 \sum_{i=1}^N (z_i - ax_i - by_i - c)(-1) = 0 \end{cases} \quad (3)$$

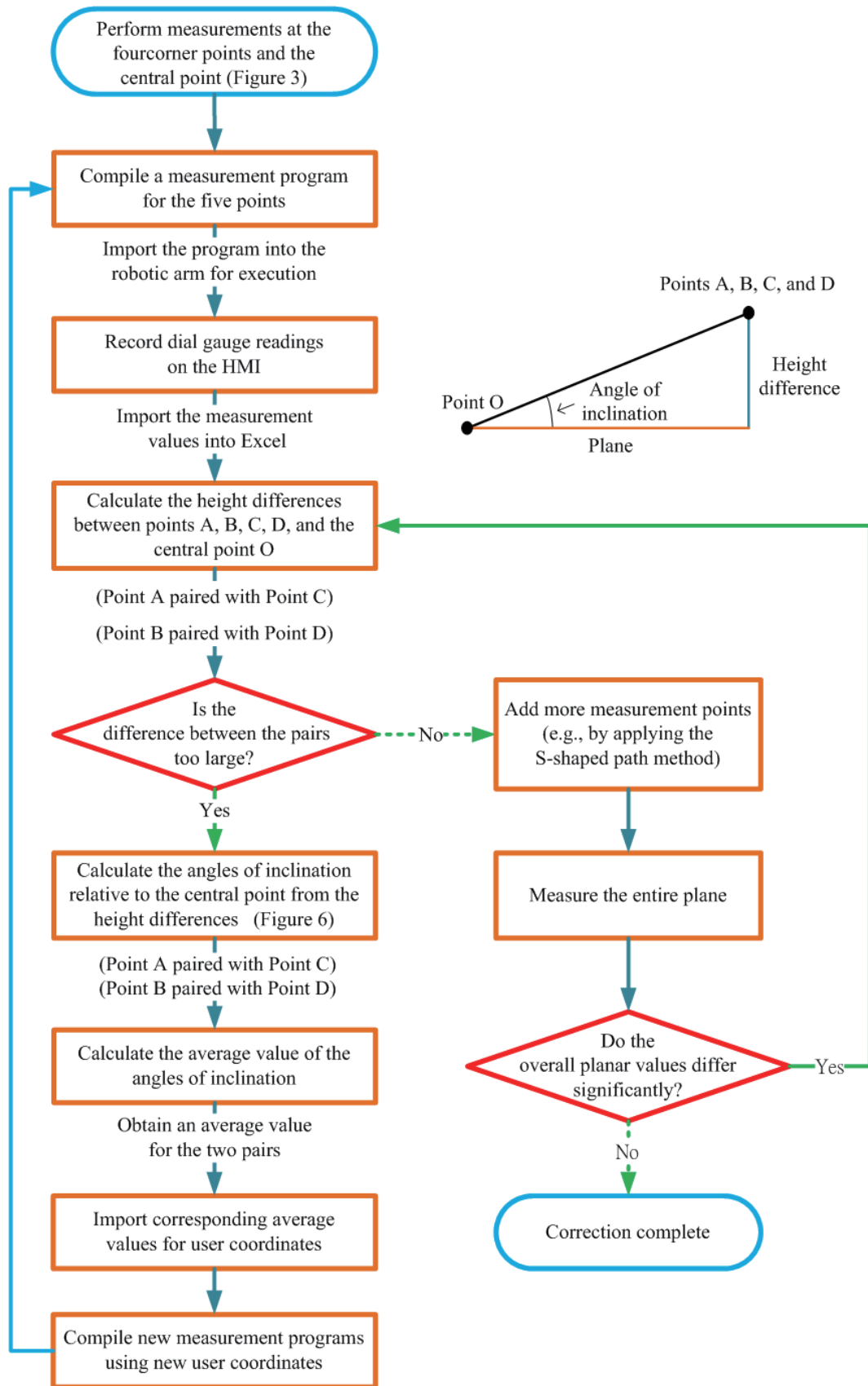


Fig. 5. (Color online) Correction process for the work surface.

Equation (3) can be reorganized into a matrix.

$$\begin{bmatrix} \sum x_i^2 & \sum x_i y_i & \sum x_i \\ \sum x_i y_i & \sum y_i^2 & \sum y_i \\ \sum x_i & \sum y_i & \sum 1 \end{bmatrix} \begin{bmatrix} a \\ b \\ c \end{bmatrix} = \begin{bmatrix} \sum x_i z_i \\ \sum y_i z_i \\ \sum z_i \end{bmatrix} \quad (4)$$

By using Eq. (4), the coefficients a , b , and c can be determined; substituting them into Eq. (1) provides the equation for the least-squares plane, and substituting them into Eq. (2) enables calculating the error for each sampled point (x_i, y_i, z_i) . The maximum positive and negative distances between the plane and sampled points are identified as $(E_i)_{max}$ and $(E_i)_{min}$, respectively; their difference is the range of the values. The flatness is

$$Error = \frac{(E_i)_{max} - (E_i)_{min}}{\sqrt{1 + a^2 + b^2}}. \quad (5)$$

If the measured surface is nearly horizontal with a and b much less than 1, then $\sqrt{1 + a^2 + b^2} \approx 1$, and Eq. (5) can be simplified as

$$Error = (E_i)_{max} - (E_i)_{min}. \quad (6)$$

4. Experimental Results

An experiment was performed in which the five-point correction method in Fig. 3 was first used to correct the work surface. The work surface was then comprehensively measured using the S-shaped path depicted in Fig. 4. The range of the values was calculated with MATLAB to quantify the flatness according to the least squares method for flatness in Sect. 3.2. This value was used to determine whether corrections were necessary; two rounds of corrections were performed. After the corrections, engraving was performed.

4.1 Measurement along the S-shaped path

Figure 4 shows the measurement points on the S-shaped path. The measurement program for these points was planned using RoboDK before it was imported into the robotic arm's teaching box. Table 2 shows the initial values for the measurement points on the S-shaped path following the five-point correction shown in Fig. 5. Figure 6 shows a depiction of the measured values along the S-shaped path: (a) initially, (b) first correction, (c) second correction, and (d) second correction for 3D colored surface [20]. From S0 to S3 ($x = -202.5$ to $x = 202.5$), the range in the x -direction increased from 5.3531 to 5.6221, 5.8001, and 5.8715, indicating that the entire work surface had a tilt. The range in the y -direction varied from 0.5596 to 0.8813, suggesting a slight incline. Table 3 shows the flatness values calculated by the least squares method in Sect. 3.2.

Table 2
(Color online) Initial values for the measurement points on the S-shaped path.

Original	S0	S1	S2	S3	U:mm
<i>X</i>	<i>Y</i>				Range <i>Y</i>
	-165	-55	55	165	
-202.5	-0.208	-0.405	-0.315	0.1546	0.5596
-157.5	0.3383	0.1839	0.2998	0.7732	0.5893
-112.5	0.9185	0.7911	0.98	1.3827	0.5916
-67.5	1.5246	1.4647	1.5573	2.0635	0.5988
-22.5	2.0733	2.0758	2.2259	2.6761	0.6028
22.5	2.6497	2.6878	2.8799	3.3072	0.6575
67.5	3.266	3.2866	3.5308	3.9818	0.7158
112.5	3.87	3.9036	4.2698	4.6951	0.8251
157.5	4.4819	4.5587	4.8224	5.3363	0.8544
202.5	5.1448	5.2171	5.4852	6.0261	0.8813
Range <i>X</i>	5.3531	5.6221	5.8001	5.8715	

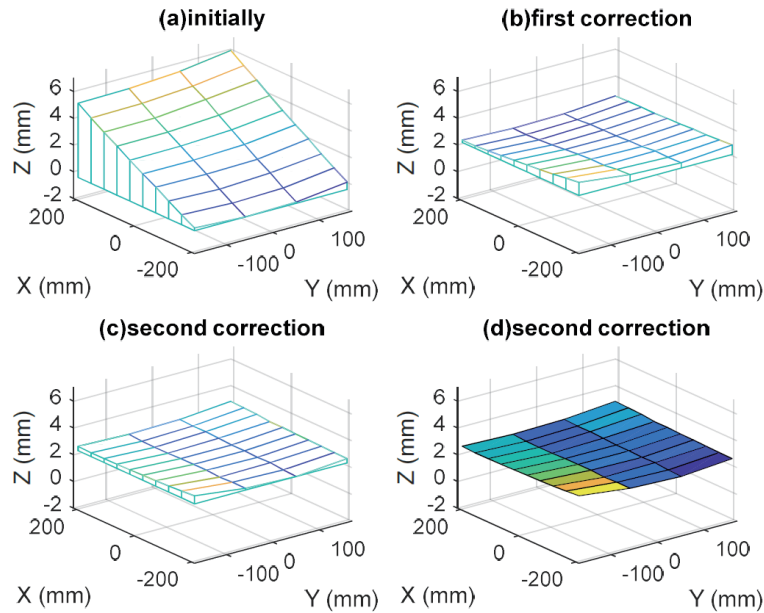


Fig. 6. (Color online) Work surface measured along the S-shaped path: (a) initially, (b) first correction, (c) second correction, and (d) second correction for 3D colored surface.

A correction was made along the *x*-axis, and Table 4 shows the resulting measurements. The flatness values and the work surface after the first correction are presented in Table 5. The work surface was still slightly tilted; the ranges for *x* and *y* were 0.8089–0.3060 and 0.5845–0.3776, respectively, at S0–S3. Therefore, a second correction was performed; the results are presented in Tables 6 and 7. The second correction decreased the ranges for *x* to 0.3099, 0.1089, 0.2881, and 0.3073; the ranges for *y* were 0.5926–0.4179. This tilt was considered acceptable.

Tables 8 and 9 show the average range and flatness values for each correction, respectively. The flatness value was smallest before the first correction (0.5414), indicating that the workpiece

Table 3
(Color online) Initially measured flatness values.

Original	S0	S1	S2	S3
<i>Y</i>				
<i>X</i>	-165	-55	55	165
-202.5	-0.339	0.0679	0.1877	-0.072
-157.5	-0.256	0.1081	0.2021	-0.061
-112.5	-0.207	0.1301	0.151	-0.042
-67.5	-0.184	0.0856	0.2028	-0.094
-22.5	-0.104	0.1036	0.1633	-0.077
22.5	-0.051	0.1207	0.1385	-0.079
67.5	-0.038	0.151	0.1167	-0.124
112.5	-0.013	0.1632	0.0068	-0.209
157.5	0.0041	0.1372	0.0833	-0.221
202.5	-0.03	0.1079	0.0497	-0.281

Table 4
(Color online) Values for the measurement points after the first correction.

First	S0	S1	S2	S3	U:mm
<i>Y</i>					
<i>X</i>	-165	-55	55	165	Range <i>Y</i>
-202.5	3.2015	2.7584	2.617	2.9267	0.5845
-157.5	3.0858	2.7062	2.5914	2.8756	0.4944
-112.5	2.9418	2.5765	2.6219	2.81	0.3653
-67.5	2.8345	2.5871	2.5108	2.7968	0.3237
-22.5	2.7425	2.5177	2.4911	2.7236	0.2514
22.5	2.6544	2.4386	2.4278	2.7106	0.2828
67.5	2.557	2.3376	2.4251	2.6564	0.3188
112.5	2.4752	2.2592	2.4094	2.6724	0.4132
157.5	2.4049	2.2215	2.315	2.6612	0.4397
202.5	2.3926	2.2431	2.3221	2.6207	0.3776
Range X	0.8089	0.5369	0.3069	0.306	

Table 5
(Color online) Flatness values after the first correction.

First	S0	S1	S2	S3
<i>Y</i>				
<i>X</i>	-165	-55	55	165
-202.5	-0.354	0.0947	0.2418	-0.062
-157.5	-0.295	0.0907	0.2112	-0.067
-112.5	-0.207	0.1642	0.1245	-0.058
-67.5	-0.156	0.0974	0.1794	-0.101
-22.5	-0.12	0.1106	0.1429	-0.084
22.5	-0.088	0.1335	0.15	-0.127
67.5	-0.047	0.1783	0.0965	-0.129
112.5	-0.021	0.2005	0.056	-0.201
157.5	-0.007	0.1819	0.0942	-0.246
202.5	-0.051	0.1041	0.0309	-0.262

Table 6

(Color online) Values for the measurement points after the second correction.

Second	S0	S1	S2	S3	U:mm
<i>X</i>	<i>Y</i>				Range <i>Y</i>
	-165	-55	55	165	
-202.5	2.9217	2.4684	2.3291	2.6419	0.5926
-157.5	2.8376	2.4832	2.381	2.6562	0.4566
-112.5	2.7758	2.4224	2.4742	2.6808	0.3534
-67.5	2.7323	2.5016	2.4364	2.7078	0.2959
-22.5	2.6968	2.4934	2.4844	2.7279	0.2435
22.5	2.6682	2.476	2.4745	2.7659	0.2914
67.5	2.6394	2.443	2.5393	2.7637	0.3207
112.5	2.6143	2.4364	2.5833	2.8723	0.4359
157.5	2.6118	2.4528	2.5688	2.9078	0.455
202.5	2.651	2.5313	2.6172	2.9492	0.4179
Range <i>X</i>	0.3099	0.1089	0.2881	0.3073	

Table 7

(Color online) Flatness values measured after the second correction.

Second	S0	S1	S2	S3
<i>X</i>	<i>Y</i>			
	-165	-55	55	165
-202.5	-0.258	0.1833	0.3101	-0.015
-157.5	-0.176	0.1663	0.256	-0.032
-112.5	-0.116	0.2248	0.1606	-0.059
-67.5	-0.075	0.1434	0.1962	-0.088
-22.5	-0.042	0.1494	0.146	-0.11
22.5	-0.015	0.1646	0.1536	-0.15
67.5	0.0115	0.1954	0.0866	-0.15
112.5	0.0343	0.1998	0.0404	-0.261
157.5	0.0346	0.1812	0.0527	-0.299
202.5	-0.007	0.1005	0.0021	-0.342

Table 8

(Color online) Comparison of the three measurements obtained by the average range method.

Original	ave. range <i>X</i>	5.6617
	ave. range <i>Y</i>	0.6876
First	ave. range <i>X</i>	0.4897
	ave. range <i>Y</i>	0.3851
Second	ave. range <i>X</i>	0.2536
	ave. range <i>Y</i>	0.3863

Table 9

Comparison of flatness values obtained by the least squares method.

Original	$\max(F) - \min(F)$	0.5414
First	$\max(F) - \min(F)$	0.5960
Second	$\max(F) - \min(F)$	0.6277

was flatter. However, the entire work surface was tilted; hence, the flatness of the work surface should not be judged solely by the least squares method. The average range should also be considered for flatness corrections. The advantages and disadvantages of the two approaches are listed in Table 10 and described as follows.

The least squares method considers the distances of all measured values and is a comprehensive flatness assessment. It is also insensitive to outliers. However, it requires far more computations than does identifying the range. Moreover, it is sensitive to measurement errors, potentially leading to inaccurate assessments.

By contrast, the range is simple to understand, use, and calculate; it only requires a comparison between the maximum and minimum values of the measured data. Its simplicity enables obtaining results rapidly. However, the result is highly sensitive to outliers because the range method only considers the maximum and minimum values. The method does not consider the distances of all measured values, causing the possible negligence of key information and resulting in less accurate assessment results.

4.2 Robotic arm engraving planning

A robotic arm engraving experiment was performed in accordance with the flowchart in Fig. 7. First, artistic images were input into the Carveco software for editing. Engraving was performed in two stages: roughing and finishing. Paths were generated for both stages and input into RoboDK to simulate robotic arm parameters and generate machining programs. When setting the robotic arm parameters, ensuring that the x -, y -, and z -directions in RoboDK align

Table 10
Advantages and disadvantages of the least squares and range methods.

	Advantages	Disadvantages
Least squares method	1. High accuracy 2. Insensitive to outliers	1. Computational complexity 2. Sensitivity to measurement errors
Range method	1. Simplicity and ease of use 2. Speed	1. Sensitivity to outliers 2. Less precise results

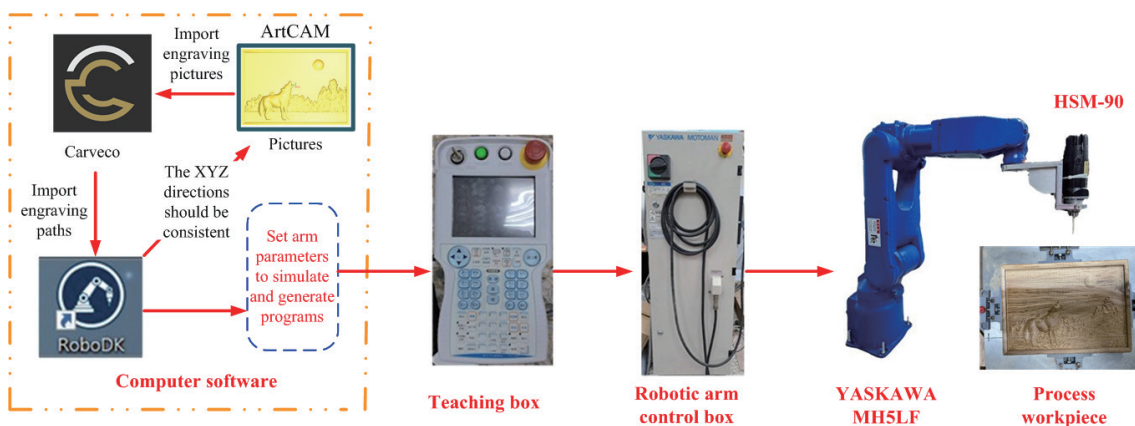


Fig. 7. (Color online) Flowchart of the equipment used for robotic arm engraving.

with those in the images is crucial. Figure 8 shows a flowchart for the software planning process. The generated engraving paths were then input into the robotic arm’s teaching box. Figure 9 shows a program flowchart for the robotic arm engraving experiment. First, the numerical control (NC) file for engraving was imported into RoboDK to adjust the angle of the machining

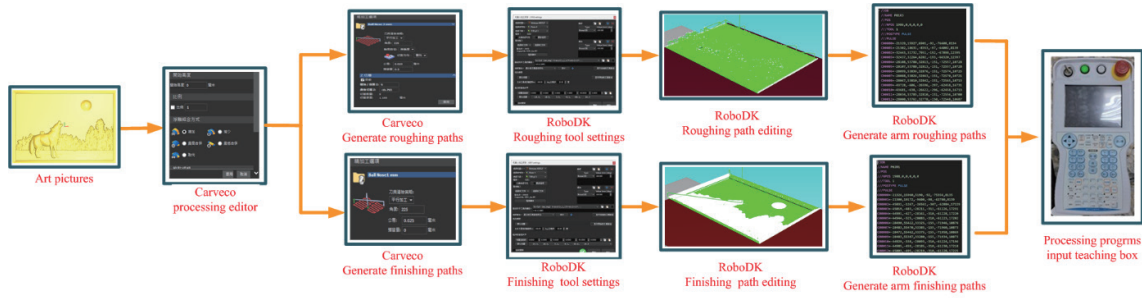


Fig. 8. (Color online) Flowchart for planning the engraving process in computer software.

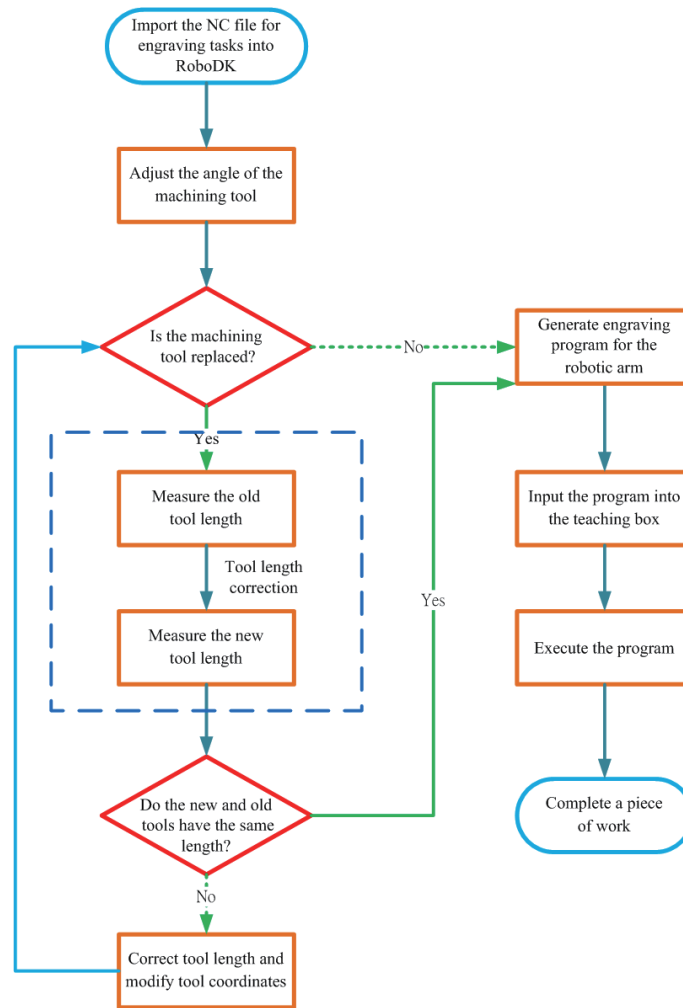


Fig. 9. (Color online) Program flowchart for the robotic arm engraving experiment.

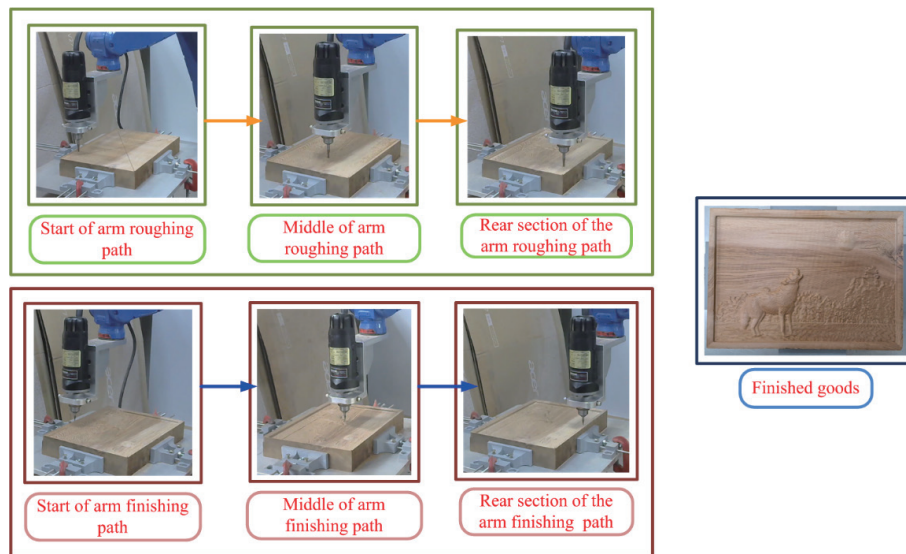


Fig. 10. (Color online) Robotic arm completing a piece of work.

tool. If there is no need to replace the tool, an engraving program is generated directly. If a tool replacement is necessary, the lengths of the old and new tools are measured; if the lengths differ, tool length correction and the modification of the tool coordinates must be performed. The engraving program is then input into the teaching box to commence roughing⁽²⁰⁾ and finishing,⁽²¹⁾ completing the engraving task. Figure 10 shows images of a robotic arm performing engraving.

5. Conclusions

In this study, we focused on correcting reference plane levelness to enhance the precision and efficiency of robotic arms in automated machining processes. By developing an automatic measurement method involving a robotic arm equipped with a mechanical probe to measure the reference plane and the RoboDK software for plane correction, we successfully achieved the correction of the machining reference plane. Furthermore, to ensure the accuracy of the correction, we conducted measurements using an S-shaped path and evaluated the machining reference plane using both flatness and range methods.

Finally, we used engraving software for machining planning and conducted actual engraving operations using the robotic arm. Through this process, we validated the stability of the robotic arm and the consistency of its machining quality as shown in Fig. 10, further verifying the effectiveness of our proposed correction method.

Overall, the automatic measurement and correction method for robotic arms proposed in this study offers a viable solution to the problem of correcting the machining reference plane levelness. This method not only improves the precision and efficiency of robotic arms in automated machining but also contributes considerably to the advancement of the manufacturing industry. In the future, we will continue to study and optimize this method to meet the growing needs of the manufacturing industry and promote its sustained development.

Acknowledgements

The authors gratefully acknowledge the financial support provided by National Pingtung University under Research Projects NPTU-AD-114-1-2, NPTU-114-010, and CCS-113-003. The support from these institutions has been essential to the successful completion of this research.

References

- 1 Y. M. Cheng, G. M. Chang, and Y. H. Chang: *Sens. Mater.* **36** (2024) 3957.
- 2 N. Elango and A. A. M. Faudzi: *Int. J. Adv. Manuf. Technol.* **80** (2015) 1027. <https://doi.org/10.1007/s00170-015-7085-3>
- 3 W. Ji and L. Wang: *Int. J. Adv. Manuf. Technol.* **103** (2019) 1239.
- 4 Y. Tian, M. Draelos, G. Tang, R. Qian, A. Kuo, J. Izatt, and K. T. Hauser: arXiv 2020, arXiv:2002.00530.
- 5 J. Denavit and R. S. Hartenberg: *Trans. ASME, J. Appl. Mech.* **77** (1955) 215.
- 6 M. M. Alam, S. Ibaraki, and K. Fukuda: *Int. J. Adv. Technol.* **15** (2021) 599. <https://doi.org/10.20965/ijat.2021.p0599>
- 7 C. J. Lin, H. C. Wang, and C. C. A. Wang: *Actuators* **12** (2023) 107. <https://doi.org/10.3390/act12030107>
- 8 C. J. Lin and H. C. Wang: *Proc. 2022 IEEE Int. Conf. Advanced Robotics and Intelligent Systems (ARIS) (IEEE, 2022)* 1. <https://doi.org/10.1109/ARIS56205.2022.9910448>
- 9 J. Hallenberg: *Robot Tool Center Point Calibration Using Computer Vision*, Dept. Electr. Eng. (Linköping Univ., Linköping, Sweden) (2007).
- 10 L. Zhang, C. Li, Y. Fan, X. Zhang, and J. Zhao: *Sensors* **21** (2021) 366. <https://doi.org/10.3390/s21020366>
- 11 S. Liu, Y. Wu, C. Qiu, and X. Zou: *Proc. 2021 2nd Int. Conf. Control, Robotics and Intelligent System (CCRIS '21) (ACM, 2021)* 244–249.
- 12 F. Fares, H. Souifi, Y. Bouslimani, and M. Ghribi: *Proc. 2021 IEEE Int. Symp. Robotic and Sensor Environments (ROSE) (IEEE, 2021)* 1–6. <https://doi.org/10.1109/ROSE52750.2021.9611759>
- 13 C. Borrmann and J. Wollnack: *Int. J. Mater. Sci. Eng.* **3** (2015) 12.
- 14 H. Xue, O. Martin, N. Southon, and N. Yu: *Proc. Laser Metrology and Machine Performance XV* (2021).
- 15 I. Kuric, V. Tlach, M. Sága, M. Císar, and I. Zajačko: *Appl. Sci.* **11** (2021) 1777. <https://doi.org/10.3390/app11041777>
- 16 G. Bergström: *Method for Calibrating of Off Line Generated Robot Program*, Master's Thesis (Chalmers Univ. Technol., Göteborg, Sweden) (2011).
- 17 Y. Cai, H. Gu, C. Li, and H. Liu: *Robot. Comput. Integr. Manuf.* **50** (2018) 276.
- 18 Y. M. Cheng: *Materials* **15** (2022) 2268. <https://doi.org/10.3390/ma15062268>
- 19 Y. M. Cheng, W. X. Peng, and A. C. Hsu: *Int. J. Adv. Manuf. Technol.* **76** (2015) 1253.
- 20 Six axis robot arm for rough machining of relief engraving: <https://www.youtube.com/watch?v=N1xqnHsvHXI> (accessed April 2024).
- 21 Six axis robotic arm for precision machining of relief engraving: <https://www.youtube.com/watch?v=8eTjd0WUho&t=10s> (accessed April 2024).